Research Article | Vol. 29, No. 18 / 30 Aug 2021 / Optics Express 28329
Optics EXPRESS

Lossless dielectric metasurface with giant intrinsic chirality for terahertz wave

JIE LI,[1] JITAO LI,[1] CHENGLONG ZHENG,[1] YUE YANG,[1] ZHEN YUE,[1] XUANRUO HAO,[1] HONGLIANG ZHAO,[1] FUYU LI,[2] TINGTING TANG,[2] LIANG WU,[1] JINING LI,[1,*] YATING ZHANG,[1,3] AND JIANQUAN YAO[1,4]

[1]*Key Laboratory of Opto-Electronics Information Technology (Tianjin University), Ministry of Education, School of Precision Instruments and Opto-Electronics Engineering, Tianjin University, Tianjin, 300072, China*
[2]*Information Materials and Device Applications Key Laboratory of Sichuan Provincial Universities, Chengdu University of Information Technology, Chengdu 610225, China*
[3]*yating@tju.edu.cn*
[4]*jqyao@tju.edu.cn*
[*]*jiningli@tju.edu.cn*

Abstract: It is difficult for single-layer metal metasurfaces to excite in-plane component of magnetic dipole moment, so achieving giant intrinsic optical chirality remains challenging. Fortunately, displacement current in dielectric metasurfaces can form the in-plane magnetic moment which is not orthogonal to the electric dipole moment and forms intrinsic chirality. Here, we show a lossless all-silicon metasurface which achieves giant intrinsic chirality in terahertz band. The leaky waveguide mode in the chiral silicon pillars simultaneously excite the in-plane electric and magnetic dipole moments, which triggers the spin-selected backward electromagnetic radiation, and then realizes the chiral response. The theoretical value of circular dichroism in the transmission spectrum reaches 69.4%, and the measured one is 43%. Based on the photoconductivity effect of the silicon metasurface, we demonstrate optical modulation of the intrinsic chirality using near-infrared continuous wave. In addition, by arranging the two kinds of meta-atoms which are enantiomers, we show the spin-dependent and tunable near-field image display. This simple-prepared all-silicon metasurface provides a new idea for the design of terahertz chiral meta-devices, and it is expected to be applied in the fields of terahertz polarization imaging or spectral detection.

1. Introduction

Chirality of objects is widespread in nature, such as certain galaxies in the universe, human hands, DNA molecules with double helix structure, and so on. In general, chirality refers to the fact that the object and its mirror image cannot be completely overlapped by operations such as translation and rotation [1]. The mirror image of a chiral molecule is also called the chiral enantiomer. On the other hand, the electric field oscillation trajectory of circularly polarized light exhibits a three-dimensional spiral structure, which also shows chirality. More interestingly, the chirality of light beam and optical medium show a special interaction named chiral optical responses [2]. It can be considered that chiral media have different real or imaginary parts of refractive index for the two kinds of circularly polarized light, which correspond to circular birefringence and circular dichroism (CD), respectively. The CD of light can be used to distinguish chiral enantiomers, and has a wide range of applications in the fields of biomedicine and chemical engineering [3,4]. However, it is mainly caused by electronic energy level transitions (electronic circular dichroism, ECD) or molecular vibrations (vibratory circular dichroism, VCD) in natural materials, which is very weak and requires high measurement accuracy [5]. Metasurfaces are artificially designed

#430033 https://doi.org/10.1364/OE.430033
Journal © 2021 Received 27 Apr 2021; revised 4 Aug 2021; accepted 10 Aug 2021; published 18 Aug 2021

Optics EXPRESS

two-dimensional subwavelength meta-atoms array, which show unique advantages in beam manipulation and local field enhancement [6–8]. Chiral or achiral metasurfaces may induce strong interactions between light field and chiral substances, which have been used to enhance the circular dichroism of chiral molecules [9–11].

On the other hand, manipulation of light field based on chiral metasurfaces is also extremely important. Different from the chiral metamaterials with three-dimensional spiral structure, chiral metasurfaces are easier to process, especially for the near-infrared and visible bands [12,13]. However, it is difficult for a single-layer metal meta-atoms to achieve obvious chiral responses for normal incident wave, because it can only form a conduction current in the metal plane, and thus it is difficult to generate an in-plane magnetic dipole moment [14]. To this end, several solutions have been proposed. For example, "quasi 2D" metasurfaces based on two- or even multi-layer meta-atoms are reported [15–18]. Another option is the reflective metasurface with a whole layer of metal reflector at the bottom [19–22]. This type of chiral optical phenomenon is called intrinsic chirality of optical devices. In addition, by introducing an inclination angle to the incident beam, an "in-plane" component of the magnetic dipole moment can also be excited, and then a chiral response can be observed in the higher-order beam, which is called extrinsic chirality [23–26]. In general, intrinsic chirality seems to have more application potentials. After all, application examples in chiral holography, circularly polarized light detection, wavefront manipulation, and chiral sensing have been demonstrated [27–35]. Therefore, metasurfaces with simple structures and high-efficiency intrinsic chirality may be an extremely important research topic. Different from the single-layer metal structures, the lossless dielectric metasurface may form a displacement current inside the meta-atoms, which in turn generates an in-plane magnetic dipole moment. Capasso's group used high-order dipoles in dielectric nanostructures to achieve huge CD in visible band [36]. Dielectric chiral metasurfaces for near-infrared wave have also been proposed by several groups [37,38]. In terahertz band, the above-mentioned scheme of processing high refractive index meta-atoms on low refractive index substrates is difficult because the required deposition thickness of upper material is very thick. Although bonding or adhesion can also be used to achieve a similar structure, it is complicated and the thickness is not easy to control [39].

Here, we propose a scheme for high-efficiency terahertz intrinsic chirality based on all-silicon metasurface. Using the meta-device obtained by only a single deep etching of silicon, giant CD in the transmission spectrum is observed, which is attributed to the in-plane magnetic dipole moment formed by the guided mode resonance. Based on this simple structure, we also demonstrate its all-optical tunability. The 1064 nm continuous laser beam can form uniformly distributed photo-generated carriers in high-resistance silicon, thereby absorbing the incident terahertz waves and weaken the chirality. In addition, we use the meta-enantiomers to achieve a tunable image display in the transmitted near field.

2. Results and discussion

In terahertz band, all-silicon metasurface is a new solution for high-efficiency wavefront manipulation [40], which with a simple preparation process. High-resistance silicon shows high refractive index and negligible loss or dispersion, while the leaky waveguide mode in the meta-atoms can achieve efficient control of phase and polarization of terahertz wave. Here we hope to show the new features of all-silicon meta-devices. The chiral metasurface is shown in Fig. 1, in which the devices composed of two kinds of chiral enantiomers can selectively reflect or transmit different circularly polarized waves. According to design rule of the reflective CD in metasurface, the meta-atoms need to break both the mirror symmetry and the n-th order rotational symmetry (C_n, $n>2$) [19]. Therefore, we choose the structure in Fig. 1, which is equivalent to two specially placed "L"-shaped silicon pillars and satisfies the above-mentioned symmetry conditions. Using numerical simulation software (CST 2019, MICROWAVE STUDIO) for

Optics EXPRESS

parameter optimization, we obtain the final structure size as follows. The height of the silicon pillar is H=200 μm, and L=60 μm,W=70 μm, the outer contour of the unit is equivalent to an elliptical column, with a long axis of 180 μm and short axis of 120 μm. The period is P=200 μm, and thickness of the substrate is 300 μm.

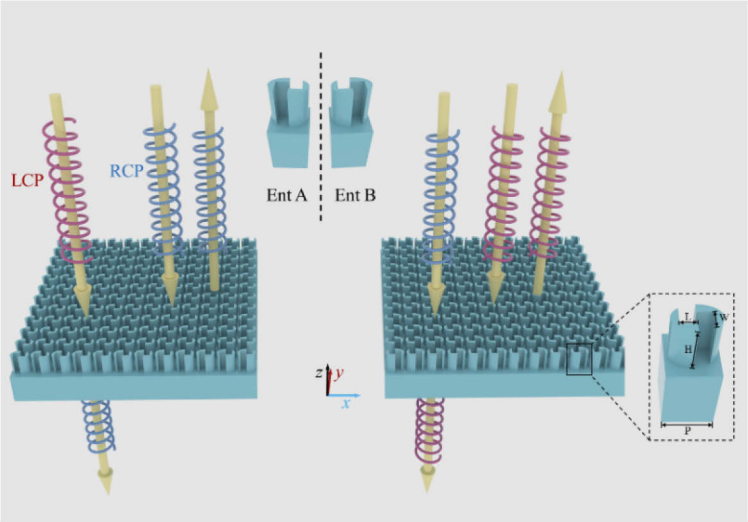

Fig. 1. A schematic diagram of the all-silicon metasurfaces with giant intrinsic chirality.

We simulate the transmission spectrum of the metasurface with time-domain solver, in which both x and y directions are set as periodic boundary conditions, and z direction is set as open conditions. We add x- or y-polarized plane waves as the excitation source, and the linear polarization components in the transmitted wave are detected by a probe. Then we use the following equations to calculate the four transmission coefficients of circular polarizations and the transmitted circular dichroism (T_{CD}) [41]:

$$\begin{pmatrix} r_{\mathrm{RR}} & r_{\mathrm{RL}} \\ r_{\mathrm{LR}} & r_{\mathrm{LL}} \end{pmatrix} = \frac{1}{2}\begin{pmatrix} r_{xx}+r_{yy}+i(r_{xy}-r_{yx}) & r_{xx}-r_{yy}-i(r_{xy}+r_{yx}) \\ r_{xx}-r_{yy}+i(r_{xy}+r_{yx}) & r_{xx}+r_{yy}-i(r_{xy}-r_{yx}) \end{pmatrix} \tag{1}$$

$$T_{\mathrm{CD}} = T_{\mathrm{R}} - T_{\mathrm{L}} = |t_{\mathrm{RR}}|^2 + |t_{\mathrm{LR}}|^2 - (|t_{\mathrm{LL}}|^2 + |t_{\mathrm{RL}}|^2). \tag{2}$$

Based on the structural parameters in Fig. 1, we fabricate the metasurface samples (sample A and sample B consist of Ent A and Ent B, respectively) by using inductively coupled plasma (ICP) etching technology on commercial silicon wafers with a thickness of 500 μm. The optical path for measurement is shown in Fig. 2(a). Since the commonly used terahertz time-domain spectroscopy (TDS) system cannot directly measure the polarization component orthogonal to the incident wave, we need to use four metal wire grid polarizers [42]. During the measurement, the polarization directions of P1 and P3 are kept consistent with the polarization of the transmitting and receiving antennas respectively, and then P2 and P4 are rotated in turn, while taking the ±45 degrees as the new reference coordinate axes. After the four transmission coefficient components are obtained, the circular polarizations are calculated according to Eq. (1). The scanning electron micrograph (SEM) image of sample A is shown in Fig. 2(b). The simulation results of the circular polarization coefficients and CD spectrum of the two metasurfaces are shown in Figs. 2(c)-(e). It can be seen that co-polarizations of the two samples are very small (about 0.1) near the working frequency of 1THz, while the two cross-polarization components are 0.7 and 0.35, respectively.

Optics EXPRESS

It is worth mentioning that the first-order transmission coefficient of the silicon barrier is 0.7, so the parameters we selected have been able to achieve a significant difference of circular polarized waves in transmission. According to the Eq. (2), we calculate the transmission CD spectra of the two samples. From Fig. 2(e), it can be found that the peak value of CD reaches ±0.34. We define the ratio of CD to first-order transmission of the silicon wafer as the efficiency

$$\eta = \frac{T_{\mathrm{CD}}}{T_{\mathrm{Si}}}. \tag{3}$$

Therefore, theoretical peak value of the efficiency in Fig. 2 is 69.4%, while the measured results are shown in Figs. 2(f)-(h). Their variation rules are basically agree with the simulation results, except that there is a slight attenuation in amplitude and a frequency shift of about 0.1 THz. This may be caused by the etching deviation of the sample. Carefully observing the SEM image, we find that the lateral dimension of the meta-atom is slightly different from the design value. The significant measurement errors in the high-frequency region (1.3-1.6 THz) in Figs. 2(f) and 2(g) may be caused by the low signal-to-noise ratio of the terahertz signals transmitted by the polarizers. In addition, rotating the polarizer multiple times during the measurement may also introduce deviations. The maximum value of measured T_{CD} in Fig. 2(h) is -0.21, and its efficiency is about 43%.

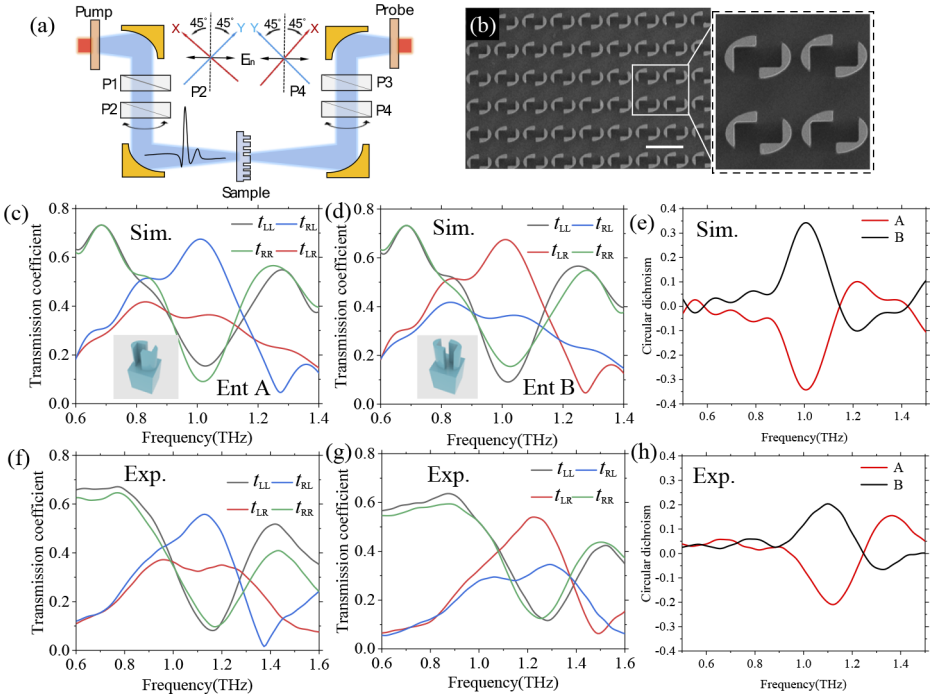

Fig. 2. Simulation and experimental results of circular dichroism in the metasurfaces. (a) Schematic of the experimental setup for transmission spectrum measurement. (b) SEM images of the metasurface sample (Ent A). (c)-(e) Simulation and (f)-(h) experimental results of the circular polarization transmission coefficients and CD spectrum for chiral enantiomers A and B.

In order to explain the physical mechanism of the giant intrinsic chirality in Fig. 2, we calculate the electromagnetic field distributions of the meta-atoms when two circularly polarized waves are incident (f=1 THz), as shown in Fig. 3(a). Figures 3(a_1) and 3(a_2) show the localized electric and magnetic fields when RCP wave is incident. Since the height of the silicon pillar is 200

Optics EXPRESS

μm and the substrate has the same refractive index, it is difficult to form standard electric and magnetic dipoles in the unit, while a waveguide mode is actually formed. But this does not affect the excitation of in-plane electric and magnetic dipole moments, which can produce efficient back scattering. When LCP wave is incident, Figs. 3(a_3) and 3(a_4) show almost no enhanced electric or magnetic fields, which means high transmittance. In order to further show the electromagnetic field distributions, we give the results in horizontal section in Figs. 3(a_5)–3(a_8). Obviously, the field distributions in the z-axis direction in these figures are not simple electric or magnetic poles, which also shows that these units act as truncated waveguides. In addition, we simulate the reflected and transmitted electric fields of the meta-atomic array to further verify that the transmitted circular dichroism is caused by spin selective reflection, which is shown in Fig. 3(b). It can be seen that the co-polarized components in transmitted waves are very small. When RCP wave is incident, the reflected co-polarization component can be seen clearly in Fig. 3(b_1), and the transmitted cross-polarization is much smaller than that in Fig. 3(b_4). The reflected and incident LCP waves can be separated, after all, their E_x and E_y (electric field components) have different phase differences. The distributions of these electromagnetic fields are consistent with the transmission spectrum in Fig. 2.

The dynamic tunability of chiral metasurfaces is also a very interesting topic, since tunable chiral meta-devices for terahertz wave based on light, electric or thermal fields have been reported. Here we show a simple modulation method of the chiral metasurface using low-power continuous laser. As shown in Fig. 4(a), we introduce an obliquely incident continuous wave of 1064 nm on the sample, since the optical path of the terahertz wave is placed in a transparent box and a normal incidence of the laser is difficult to achieve. As we all know, high-resistance silicon shows efficient transmission and weak absorption for the working wavelength, so the laser beam can cover the entire sample thickness range. A uniform distribution of photogenerated carriers is obtained inside, which causes a giant absorption of incident terahertz wave. To this end, we have carried out experimental verification, taking the transmission coefficient TLR as an example. As shown in Fig. 4(b), when the laser power is gradually increased from 0 to 650 mW, the terahertz transmission decreases significantly, while the measured time-domain signals are show in Fig. 4(c). Figures 4(d) and 4(e) show the simulation and experimental results of the transmitted CD spectrum. In order to visually demonstrate the absorption of terahertz wave by laser-irradiated samples, we show the electromagnetic field distribution in meta-atoms with different conductivity values of silicon. It can be seen from Fig. 4(f) that the reflected terahertz wave does not increase significantly but is directly dissipated inside the sample when the conductivity increases.

Based on the above-mentioned optically tunable chiral meta-atoms (enantiomers), we demonstrate a transmissive and tunable image display in near-field region, reflections of which have been reported [21,22]. In Fig. 5(a), the image we choose is a five-pointed star, and the enantiomers are arranged in the manner as shown in Fig. 5(b), which contains 50×50 units. We simulate the transmitted electric field of the metasurface when different circularly polarized waves are incident, observing the electric field intensity and phase distribution at the operating frequency (1 THz). As shown in Figs. 5(c) and 5(g), the transmitted electric fields (700 μm from the upper surface) are patterns of two complementary five-pointed stars, in which the electric field inside and around the five-pointed star is obviously different. The phases shown in Figs. 5(d) and 5(h) are also complementary. When the electrical conductivity of silicon is set to be 80 S/m, the intensity of the transmitted electric field decreases sharply, and almost no clear pattern occurs, although the phase distributions seem to be stars.

Optics EXPRESS

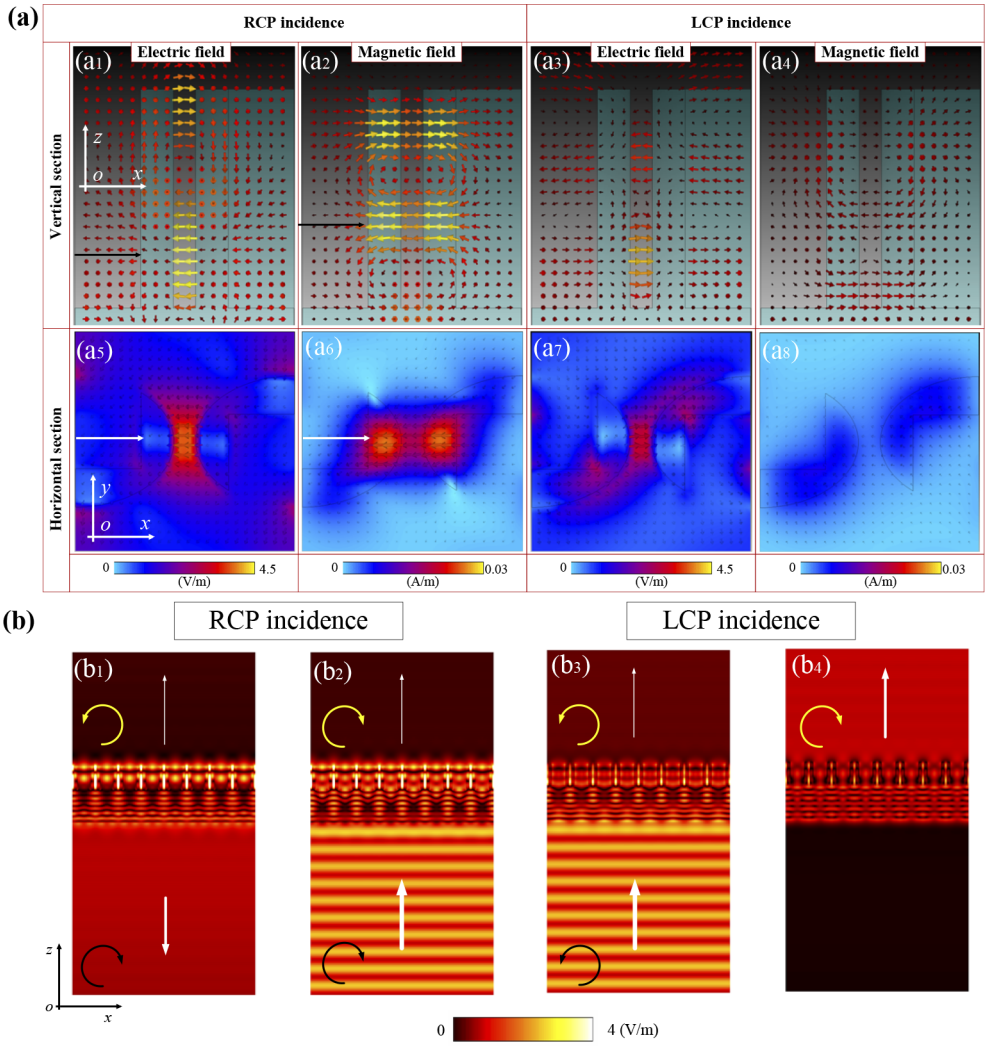

Fig. 3. Analysis of the physical mechanism for intrinsic chirality in the proposed metasuface. (a) Distributions of electric and magnetic fields in single meta-atom with different circular polarizations. (b) The electric field distributions of reflected and transmitted waves in meta-atom array.

Optics EXPRESS

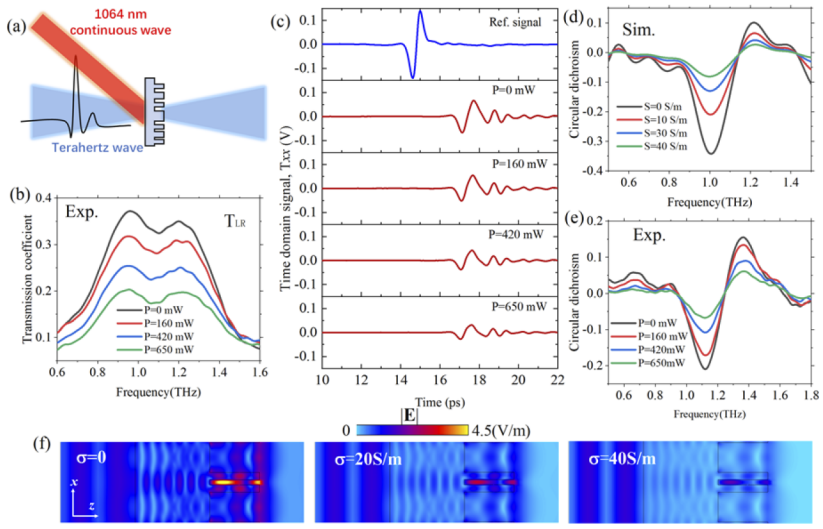

Fig. 4. Optical tunability of the chirality using near-infrared continuous wave. (a) Schematic diagram of the irradiation with infrared and terahertz wave. (b) Frequency and (c) time domain signals of the transmission coefficients (T_{LR}) under different laser powers. (d) Simulation and (e) experimental results of the optically modulated CD. (f) Electric field distributions under different conductivities of silicon.

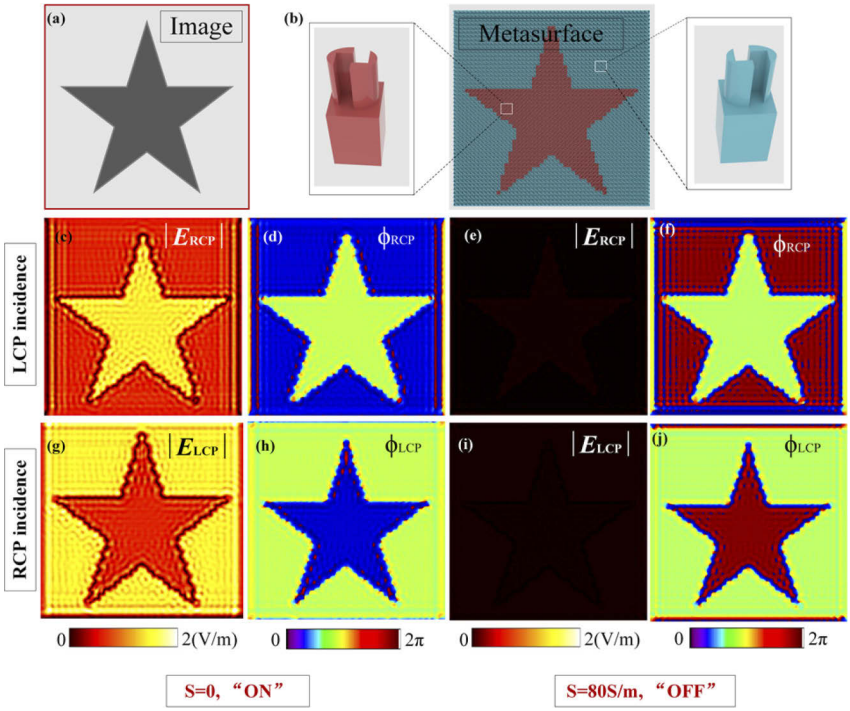

Fig. 5. Spin-dependent and tunable near-field image display based the chiral metasurface. (a) The original image we chose. (b) Arrangement of the chiral enantiomers. (c)-(j) The transmission electric field and phase distributions with different circularly polarized terahertz waves.

Optics EXPRESS

3. Conclusion

In summary, we have shown a new scheme for realizing giant intrinsic chirality of terahertz wave in the lossless dielectric metasurfaces. We calculate the transmission CD spectrum and obtain the appropriate structural parameters by using simulation software. The maximum value of T_{CD} reaches 69.4%. According to the simulated electromagnetic field distributions of the meta-atoms, we find that the giant intrinsic chirality originates from the leaky waveguide mode excited in the silicon pillars. The in-plane components of the electric and magnetic dipole moments which appear at the same time cause spin-selective back-scattering. To prove this, we simulate the electric field distributions of the reflected and transmitted waves near the metasurface. Then we prepare two metasurface samples and measured the circular polarization transmission coefficients and CD spectrum using the polarization-dependent terahertz time-domain spectroscopy system, in which the maximum T_{CD} reached 43%. In addition, we use a continuous laser with a wavelength of 1064 nm to achieve the optical modulation of the metasurface, and the transmission CD spectrum shows an efficient attenuation. As an application demonstration, we use the above-mentioned tunable chiral meta-device for switchable transmissive near-field image display. The simulation results show that the near-field pattern has high contrast and switching efficiency. This kind of chiral metasurface based on lossless dielectric is simple to prepare and is expected to be used in terahertz communications, imaging and other fields.

Funding. Basic Research Program of Shenzhen (JCYJ20170412154447469); National Key Research and Development Program of China (2017YFA0700202); National Natural Science Foundation of China (61675147, 61735010, 91838301).

Disclosures. The authors declare no conflicts of interest.

Data availability. Data underlying the results presented in this paper are not publicly available at this time but may be obtained from the authors upon reasonable request.

References

1. J. B. Pendry, "A chiral route to negative refraction," Science **306**(5700), 1353–1355 (2004).
2. M. Schäferling, *Chiral Nanophotonics: Chiral Optical Properties of Plasmonic Systems*, *Springer Series in Optical Sciences* 205, (Springer International Publishing, 2017).
3. J. Lu, Y. Xue, K. Bernardino, N. Zhang, W. R. Gomes, N. S. Ramesar, S. Liu, Z. Hu, T. Sun, A. F. de Moura, N. A. Kotov, and K. Liu, "Enhanced optical asymmetry in supramolecular chiroplasmonic assemblies with long-range order," Science **371**(6536), 1368–1374 (2021).
4. L. Chen, J. Zheng, J. Feng, Q. Qian, and Y. Zhou, "Reversible modulation of plasmonic chiral signals of achiral gold nanorods using chiral supramolecular template," Chem. Commun. **55**(76), 11378–11381 (2019).
5. W. J. Choi, G. Cheng, Z. Huang, S. Zhang, T. B. Norris, and N. A. Kotov, "Terahertz circular dichroism spectroscopy of biomaterials enabled by kirigami polarization modulators," Nat. Mater. **18**(8), 820–826 (2019).
6. N. Yu, P. Genevet, M. A. Kats, F. Aieta, J.-P. Tetienne, F. Capasso, and Z. Gaburro, "Light Propagation with Phase Discontinuities: Generalized Laws of Reflection and Refraction," Science **334**(6054), 333–337 (2011).
7. N. Yu and F. Capasso, "Flat optics with designer metasurfaces," Nat. Mater. **13**(2), 139–150 (2014).
8. S. Sun, Q. He, S. Xiao, Q. Xu, X. Li, and L. Zhou, "Gradient-index meta-surfaces as a bridge linking propagating waves and surface waves," Nat. Mater. **11**(5), 426–431 (2012).
9. N. A. Abdulrahman, Z. Fan, T. Tonooka, S. M. Kelly, N. Gadegaard, E. Hendry, A. O. Govorov, and M. Kadodwala, "Induced Chirality through Electromagnetic Coupling between Chiral Molecular Layers and Plasmonic Nanostructures," Nano Lett. **12**(2), 977–983 (2012).
10. J. García-Guirado, M. Svedendahl, J. Puigdollers, and R. Quidant, "Enhanced Chiral Sensing with Dielectric Nanoresonators," Nano Lett. **20**(1), 585–591 (2020).
11. M. L. Solomon, J. Hu, M. Lawrence, A. García-Etxarri, and J. A. Dionne, "Enantiospecific Optical Enhancement of Chiral Sensing and Separation with Dielectric Metasurfaces," ACS Photonics **6**(1), 43–49 (2019).
12. V. K. Valev, J. J. Baumberg, C. Sibilia, and T. Verbiest, "Chirality and chiroptical effects in plasmonic nanostructures: fundamentals, recent progress, and outlook," Adv. Mater. **25**(18), 2517–2534 (2013).
13. Z. Wang, F. Cheng, T. Winsor, and Y. Liu, "Optical chiral metamaterials: a review of the fundamentals, fabrication methods and applications," Nanotechnology **27**(41), 412001 (2016).
14. S. Yoo and Q. Park, "Chiral Light-Matter Interaction in Optical Resonators," Phys. Rev. Lett. **114**(20), 203003 (2015).
15. J. Mun, M. Kim, Y. Yang, T. Badloe, J. Ni, Y. Chen, C.-W. Qiu, and J. Rho, "Electromagnetic chirality: from fundamentals to nontraditional chiroptical phenomena," Light Sci Appl **9**(1), 139 (2020).
16. S. P. Rodrigues, S. Lan, L. Kang, Y. Cui, P. W. Panuski, S. Wang, A. M. Urbas, and W. Cai, "Intensity-dependent modulation of optically active signals in a chiral metamaterial," Nat Commun **8**(1), 14602 (2017).

Optics EXPRESS

17. K. Tanaka, D. Arslan, S. Fasold, M. Steinert, J. Sautter, M. Falkner, T. Pertsch, M. Decker, and I. Staude, "Chiral Bilayer All-Dielectric Metasurfaces," ACS Nano **14**(11), 15926–15935 (2020).
18. F. Neubrech, M. Hentschel, and Na Liu, "Reconfigurable Plasmonic Chirality: Fundamentals and Applications," Adv. Mater **32**(41), 1905640 (2020).
19. Z. Wang, H. Jia, K. Yao, W. Cai, H. Chen, and Y. Liu, "Circular Dichroism Metamirrors with Near-Perfect Extinction," ACS Photonics **3**(11), 2096–2101 (2016).
20. H.-X. Xu, G. Hu, Y. Li, L. Han, J. Zhao, Y. Sun, F. Yuan, G.-M. Wang, Z. H. Jiang, X. Ling, T. Cui, and C.-W. Qiu, "Interference-assisted kaleidoscopic meta-plexer for arbitrary spin-wavefront manipulation," Light Sci Appl **8**(1), 3 (2019).
21. W. Ma, F. Cheng, and Y. Liu, "Deep-Learning-Enabled On-Demand Design of Chiral Metamaterials," ACS Nano **12**(6), 6326–6334 (2018).
22. L. Kang, S. P. Rodrigues, M. Taghinejad, S. Lan, K. Lee, Y. Liu, D. H. Werner, A. Urbas, and W. Cai, "Preserving Spin States upon Reflection: Linear and Nonlinear Responses of a Chiral Meta-Mirror," Nano Lett. **17**(11), 7102–7109 (2017).
23. E. Plum, V. A. Fedotov, and N. I. Zheludev, "Metamaterials: Optical Activity Without Chirality," Phys. Rev. Lett. **102**(11), 113902 (2009).
24. I. Sersic, M. Anne van de Haar, F. B. Arango, and A. F. Koenderink, "Ubiquity of Optical Activity in Planar Metamaterial Scatterers," Phys. Rev. Lett. **108**(22), 223903 (2012).
25. L. Mao, K. Liu, S. Zhang, and T. Cao, "Extrinsically 2D-Chiral Metamirror in Near-Infrared Region," ACS Photonics **7**(2), 375–383 (2020).
26. S. Yang, Y. Li, X. Chen, Q. Yang, J. Han, and W. Zhang, "Extrinsic optical activity in all-dielectric terahertz metamaterial," Opt. Lett. **45**(22), 6146–6149 (2020).
27. W. Li, Z. J. Coppens, L. V. Besteiro, W. Wang, A. O. Govorov, and J. Valentine, "Circularly polarized light detection with hot electrons in chiral plasmonic metamaterials," Nat. Commun. **6**(1), 8379 (2015).
28. Q. Wang, E. Plum, Q. Yang, X. Zhang, Q. Xu, Y. Xu, J. Han, and W. Zhang, "Reflective chiral meta-holography: multiplexing holograms for circularly polarized waves," Light: Sci. Appl. **7**(1), 25 (2018).
29. J. Li, Y. Zhang, J. Li, X. Yan, L. Liang, Z. Zhang, J. Huang, J. Li, Y. Yang, and J. Yao, "Amplitude modulation of anomalously reflected terahertz beams using all-optical active Pancharatnam-Berry coding metasurfaces," Nanoscale **11**(12), 5746–5753 (2019).
30. Z. Cao, H. Gao, M. Qiu, W. Jin, S. Deng, K.-Y. Wong, and D. Lei, "Chirality Transfer from Sub-Nanometer Biochemical Molecules to Sub-Micrometer Plasmonic Metastructures: Physiochemical Mechanisms, Biosensing, and Bioimaging Opportunities," Adv. Mater. **32**(41), 1907151 (2020).
31. F. Zhang, M. Pu, X. Li, P. Gao, X. Ma, J. Luo, H. Yu, and X. Luo, "All-Dielectric Metasurfaces for Simultaneous Giant Circular Asymmetric Transmission and Wavefront Shaping Based on Asymmetric Photonic Spin-Orbit Interactions," Adv. Funct. Mater. **27**(47), 1704295 (2017).
32. Y. Guo, M. Pu, Z. Zhao, Y. Wang, J. Jin, P. Gao, X. Li, X. Ma, and X. Luo, "Merging plasmonic and geometric phase in continuously shaped metasurfaces for arbitrary orbital angular momentum," ACS Photonics **3**(11), 2022–2029 (2016).
33. C. Wang, Z. Li, R. Pan, W. Liu, H. Cheng, J. Li, W. Zhou, J. Tian, and S. Chen, "Giant Intrinsic Chirality in Curled Metasurfaces," ACS Photonics **7**(12), 3415–3422 (2020).
34. H. Xu, G. Hu, L. Han, M. Jiang, Y. Huang, Y. Li, X. Yang, X. Ling, L. Chen, J. Zhao, and C. Qiu, "Chirality-Assisted High-Efficiency Metasurfaces with Independent Control of Phase, Amplitude, and Polarization," Adv. Optical Mater. **7**(4), 1801479 (2018).
35. H. Xu, G. Wang, M. Qi, T. Cai, and T. Cui, "Compact dual-band circular polarizer using twisted Hilbert-shaped chiral metamaterial," Opt. Express **21**(21), 24912 (2013).
36. A. Y Zhu, W. T. Chen, A. Zaidi, Y.-W. Huang, M. Khorasaninejad, V. Sanjeev, C.-W. Qiu, and Federico Capasso, "Giant intrinsic chiro-optical activity in planar dielectric nanostructures," Light Sci Appl **7**(2), 17158 (2018).
37. B. Semnani, J. Flannery, R. Al Maruf, and M. Bajcsy, "Spin-preserving chiral photonic crystal mirror," Light Sci Appl **9**(1), 23 (2020).
38. Z. Ma, Y. Li, Y. Li, Y. Gong, S. A. Maier, and M. Hong, "All-dielectric planar chiral metasurface with gradient geometric phase," Opt. Express **26**(5), 6067–6078 (2018).
39. Z. Ma, S. M. Hanham, P. Albella, B. Ng, H. Tzu Lu, Y. Gong, S. A. Maier, and M. Hong, "Terahertz All-Dielectric Magnetic Mirror Metasurfaces," ACS Photonics **3**(6), 1010–1018 (2016).
40. J. Li, C. Zheng, G. Wang, J. Li, H. Zhao, Y. Yang, Z. Zhang, M. Yang, L. Wu, J. Li, Y. Zhang, Y. Zhang, and J. Yao, "Circular dichroism-like response of terahertz wave caused by phase manipulation via all-silicon metasurface," Photon. Res. **9**(4), 567–573 (2021).
41. C. Menzel, C. Rockstuhl, and F. Lederer, "Advanced Jones calculus for the classification of periodic metamaterials," Phys. Rev. A **82**(5), 053811 (2010).
42. S. Li, M. Wei, X. Feng, Q. Wang, Q. Xu, Y. Xu, L. Liu, C. Ouyang, W. Zhang, C. Hu, X. Zhang, J. Han, and W. Zhang, "Polarization-insensitive tunable terahertz polarization rotator," Opt. Express **27**(12), 16966–16974 (2019).